Preliminary results of animal's lymphatic system study at the ANGIOGRAPHY station of the VEPP-3 storage ring

K.A.Kolesnikov[a], R.Yu. Kozlov[a], G.N.Kulipanov[a], M.V.Kuzin[a], N.A.Mezentsev[a], S.I.Nesterov[a], V.F.Pindyurin[a], G.N.Dragun[b], O.A.Rozenberg[b] and E.L.Zelentsov[b]

(a) *Budker Institute of Nuclear Physics, 630090 Novosibirsk, Russia*

(b) *Medical Tomographic Centre, 630090 Novosibirsk, Russia*

Abstract

Some recent results on testing the special double one-coordinate X-ray detector for digital subtraction angiography on synchrotron radiation from the VEPP-3 storage ring are presented. The obtained spatial resolution of the detector is in the range of 0.1-2.0 mm, which gives the possibility to investigate the limphatic nodes of animals after injection of an iodine containing contrast agent. In preliminary experiments the mediastinum limphatic nodes of alive rats were visualized at low iodine concentration.

I. INTRODUCTION

According literature data, questions concerning early diagnostics of disorders of thoraxic organs and the abdominal cavity, and, especially, the differential diagnostics of inflammatory and neoplastic diseases and metastatic spread have not yet received due attention. At the same time, the information on the state of the lymphatic system involved in all pathological processes makes it possible to identify early cases. To solve these problems, it is necessary to apply appropriate contrast substances together with high sensitive intrascopic techniques. It seems, at present, that the application of synchrotron radiation (SR) offers unique possibilities for these purposes.

In recent years, cancer of the thoraxic organs may be referred to one of the most common diseases, whereas their examination is rather complicated because of various anatomic-physiological factors. That is why we have focused our previous studies on the lymphatic system of thorax. In 1982-1993 the works on the examination of various X-ray contrast substances (XCSs) for lymphography were done, and the dynamics of XCSs transport in the lymphatic system of mediastinum was analysed by means of X-ray fluorescence analysis and X-ray microscopy and microtomography using SR [1-8]. These studies showed a rather high degree of contrast of the lymph nodes by various XCSs that allows to visualize lymph nodes in a body by sensitive X-ray imaging technique.

Though the existing angiography station at the storage ring VEPP-3 is intended for experiments on digital subtraction angiography with SR at the K-absorption edge of iodine [9], it can be completely applied for X-ray lymphography as well. Special double-beam X-ray monochromator and double one-coordinate X-ray detector were developed for this station. The X-ray monochromator has successfully tested earlier [10], and the X-ray detector was put into operation and tested lately. A good detector performance and, especially, the achieved spatial resolution as high as 0.1 mm allowed to start the real experiments with alive animals.

This paper presents some recent results on testing the double X-ray one-coordinate detector, and first results on an X-ray visualization of mediastinum lymphatic nodes of alive rats.

II. The angiography station and the detector testing

The angiography station of the VEPP-3 storage ring is schematically shown in Fig. 1. The main components of the station are the double-beam X-ray monochromator, the object scanner and the double one-coordinate X-ray detector.

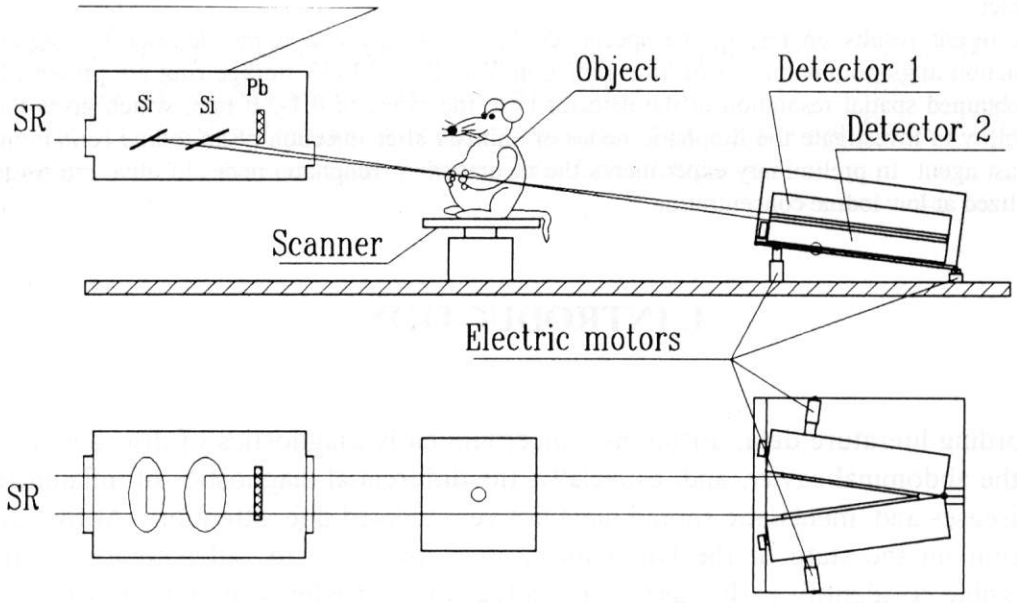

Fig. 1 Diagram of the angiography station at the VEPP-3 storage ring.

The monochromator (see Fig. 2) based on two Laue diffraction Si crystals forms two wide (10 cm) monochromatic SR beams with quanta energies just above (E_1) and below (E_2) the K-absorption edge of iodine (33.2 keV). The monochromatic beams intersect at the location of an object under study, then diverge and are detected simultaneously by the double one-coordinate X-ray detector. It means that one line of an X-ray picture is taken simultaneously at two energies of X-ray quanta. The complete subtraction picture is obtained by a vertical, line-by-line scanning of the object relative to the intersection line of monochromatic beams. The detailed descriptions of the monochromator and the detector are given in refs.[10] and [11], respectively.

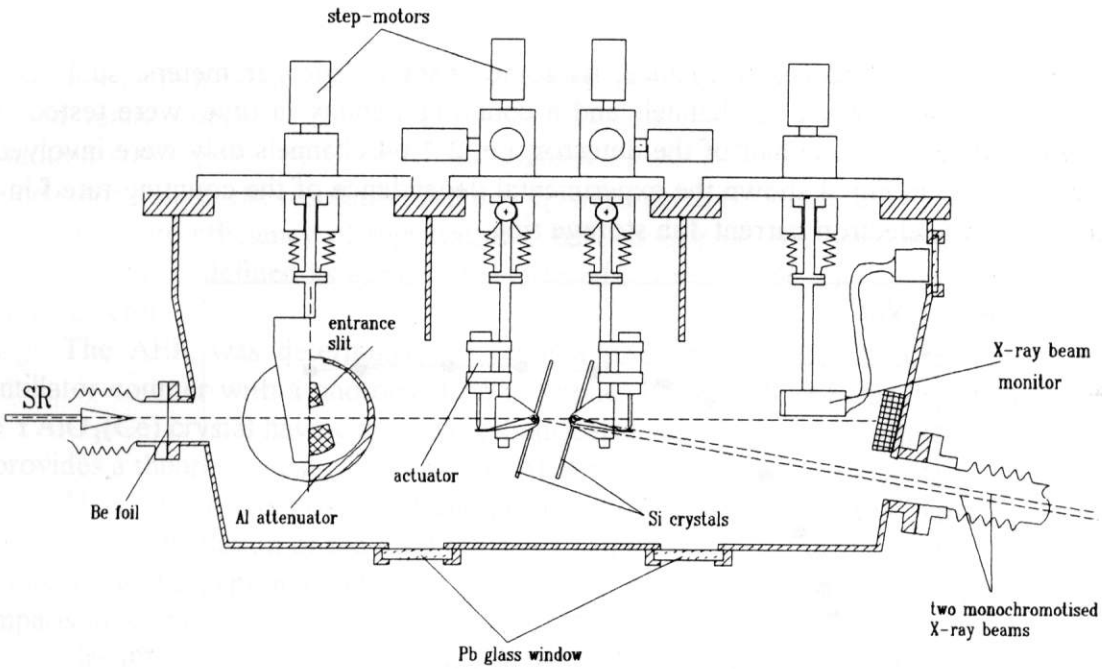

Fig. 2 Scheme of the monochromator.

The detector consists of two identical one-coordinate X-ray detectors each having 128 separate scintillation counters based on photomultipliers and $YAlO_3(Ce)$ scintillators with a decay time of about 40 ns. The detector is schematically shown in Fig. 3. The detector design allows to change its spatial resolution from 0.2 mm to 2 mm (projected values). Each channel of the detector is set to the optimal operation mode by adjusting a high voltage on a photomultiplier. Two amplitude discrimination levels for a photomultiplier signal are identical for all channels, and the ratio of these levels is 1:3 to count properly the double photon events. The operation of detector electronics is synchronized with a revolution frequency of electron bunch in the storage ring. The maximum counting rate of each channel is about 6 MHz, and, in all cases, can not exceed 8 MHz (double revolution frequency of electron bunch in the VEPP-3). The minimum registration time of the detector is determined by a sum of the data acquisition time interval and the detector data read out interval of about 70 μs.

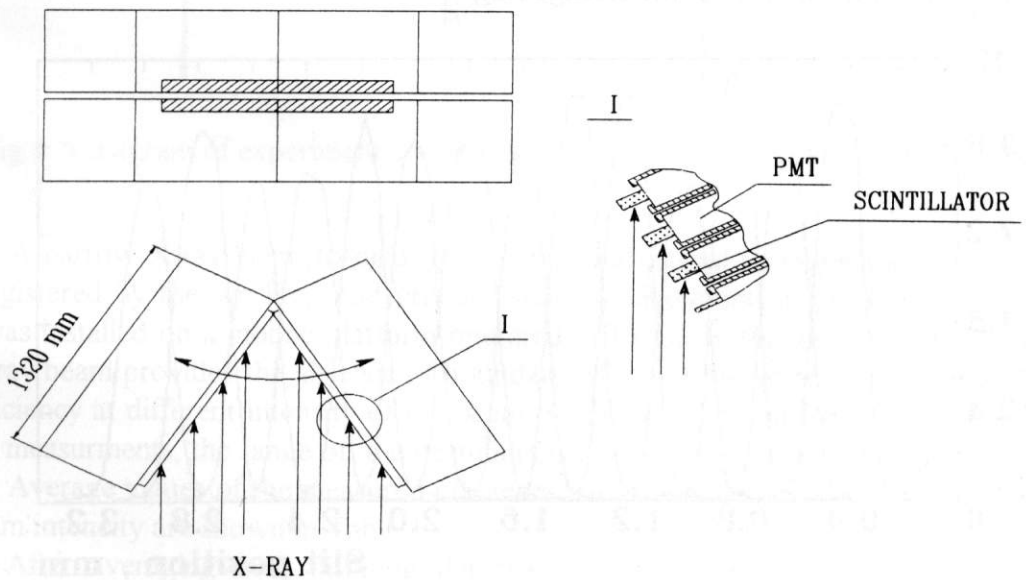

Fig. 3 Scheme of the detector and any channels

To estimate the detector performance, its some characteristic parameters, such as real spatial resolution, a homogeneity of channels and a counting stability in time, were tested. The present work was done with one half of the detector, i.e. 2 * 64 channels only were involved in the measurements, and in Fig. 4 shown the experimental dependence of the counting rate **f** in the detector channel on the electron current **J** in storage ring.

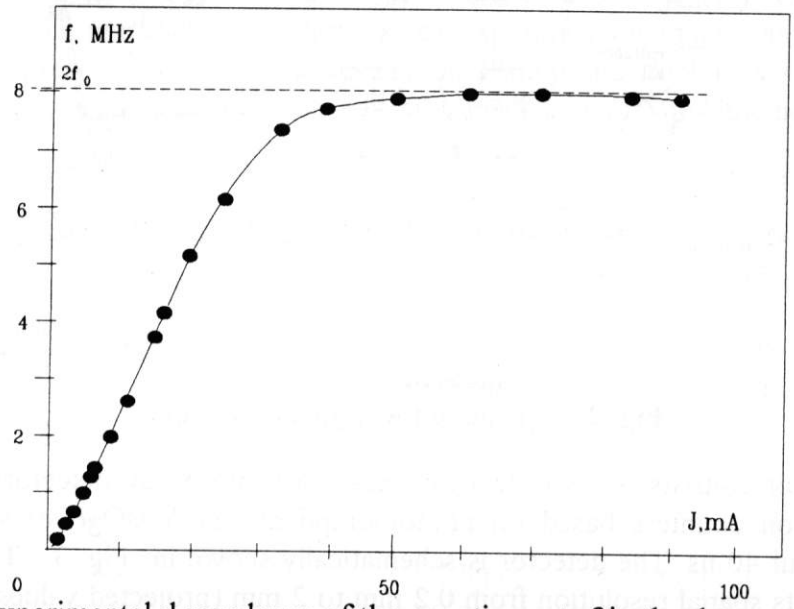

Fig. 4 Experimental dependence of the counting rate **f** in the detector channel on the electron current **J** in the storage ring.

The precision of geometric alignment of channels and the detector spatial resolution were estimated by scanning the 40 μm tantalum slit across the SR beam just in front of the detector. An example of measured profiles for 14 detector channels at the given spatial resolution of 0.2 mm is showen in Fig. 5 where the width spread of channels is about 7.3 %. The smooth shape of the profiles and appreciable tails are caused by smearing due to both a finite slit size and a finite horizontal size of the electron beam in the storage ring.

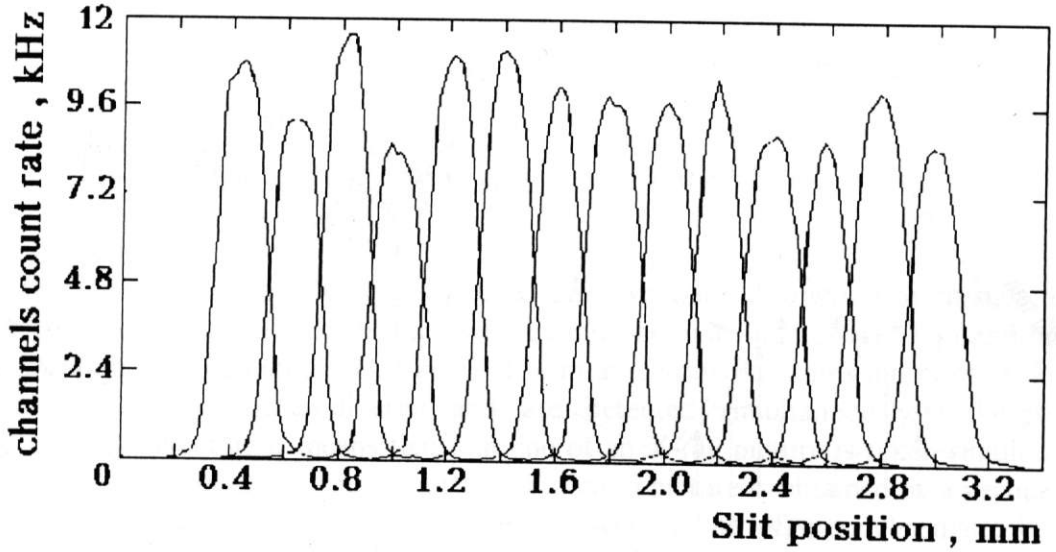

Fig.5 Example of the detector channel profiles distribution (14 channels).

It was found also, under the testing, that the spatial resolution as high as 0.1 mm can be set and really obtained instead of the 0.2 mm design value. Further increasing of spatial resolution was limited by a mechanical rigidity of the detector components and, after updating the detector design, the resolution can be improved up to 0.05 mm.

Absolute efficiency of registration (AER) is one of the basic parameters characterizing the detector. It is defined as a ratio of registered quonta to the number of quonta being incident on the detector.

The AER was determined by using a primary standard detector (PSD), based on a scintillator counter with a photoelectron multiplier PMT-130. The PSD scintillator was made of the $YAlO_3(Ce)$ crystal having a simple cylindrical shape (20 mm in diameter and 2 mm in height). It provides a theoretical calculation of the AER value with a good accuracy.

Thus, the problem of determination of the AER is divided in two parts:

1) theoretical calculation of the PSD efficiency, and then

2) measuring the experimental value of registration efficiency of the working detector using a comparison with the PSD.

The AER value for the working detector is the result of multiplication of the PSD AER value and the relative to the PSD registration efficiency of the detector.

To estimate the AER of the PSD, the processes of scattering and photoeffect in a scintillator were analysed, and the partion of quanta escaped from the crystal without their registration was estimated.

It was found in a result that theoretical value of the PSD efficiency is not less than 98,9%.

To determine the efficiency of the working detector in comparison with the PSD, the following procedure was carried out (see Fig. 6).

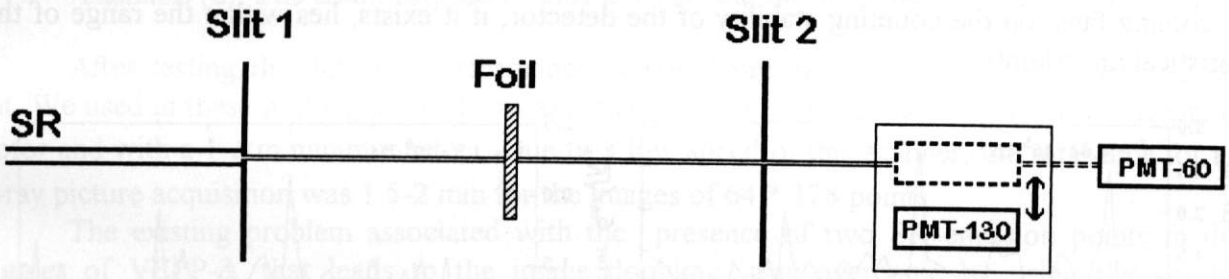

Fig.6 A diagram of experiment on the determination of the working detector efficiency.

A narrow X-ray beam formed by two slits and passed throught the foil absorbing layers was registered by the working and primary standard detectors by turns. For this purpose, the PSD was installed on a mobile platform operated under the computer control. The small size of the X-ray beam provides the absence of boundary effects in the scintillator crystal. To determine the efficiency at different intensity of the beam, a number of the absorbing foil layers was varied and, in measurments, the range of the beam intensity was from 200 to 800 kHz.

Average values of the measured efficiency for several detector channels in dependence on the beam intencity are shown in Table 1.

After averaging over different detector channels, the value of the working detector relative efficiency in comparison with the PSD was found to be 90.5%.

Thus, the AER of the working detector (the result of multiplication of the primary standard detector AER and the working detector relative efficiency) is not less than 89.5%.

TABLE 1. Averaged values of efficiency over intensity for several detectors.

Number of detector	1	2	3	4	5	6
efficiency, %	94.8	88.2	89.1	93.3	90.7	87.1

Special attention at the testing was paid to the counting stability of the detector channels because the level of instability determines the ultimate sensitivity in an X-ray imaging. The possible counting instability can be caused by many factors : an incorrect operation of the detector channels, instabilities of electron beam in the storage ring, vibration of different components of the station and so on. Figure 7 shows the normalized counting spreads $\sigma_{ch} \ / \ \sqrt{N_{ch}}$ for each of the 64 detector channels at different counting rates, data acquisition times and sampling intervals, where σ_{ch} is a standard deviation of the counting determined by 128 measurements, and N_{ch} is a mean value of the counting. It is seen in Figures 7a and 7b that, in the average, the ratio $\sigma_{ch} \ / \ \sqrt{N_{ch}}$ lies within the range of 1.0-1.5. This means, the measured counting spreads are very close to the expected ones determined by Poisson statistics, and evidences a good performance of the detector and the absence of essential disturbing factors at the station. The exclusions are several detector channels for which this ratio is somewhat higher, and these channels are the subjects for an additional adjustment. The spread distribution of Figure 7c looks like more stable with a value of the ratio less than unity, but this is due to a saturation of count rate dependence at the level of 8 MHz [11]. It was found also that the possible influence of scattered light in the experimental hall and the detector vibrations, produced by cooling fans, on the counting stability of the detector, if it exists, lies within the range of the statistical uncertainty.

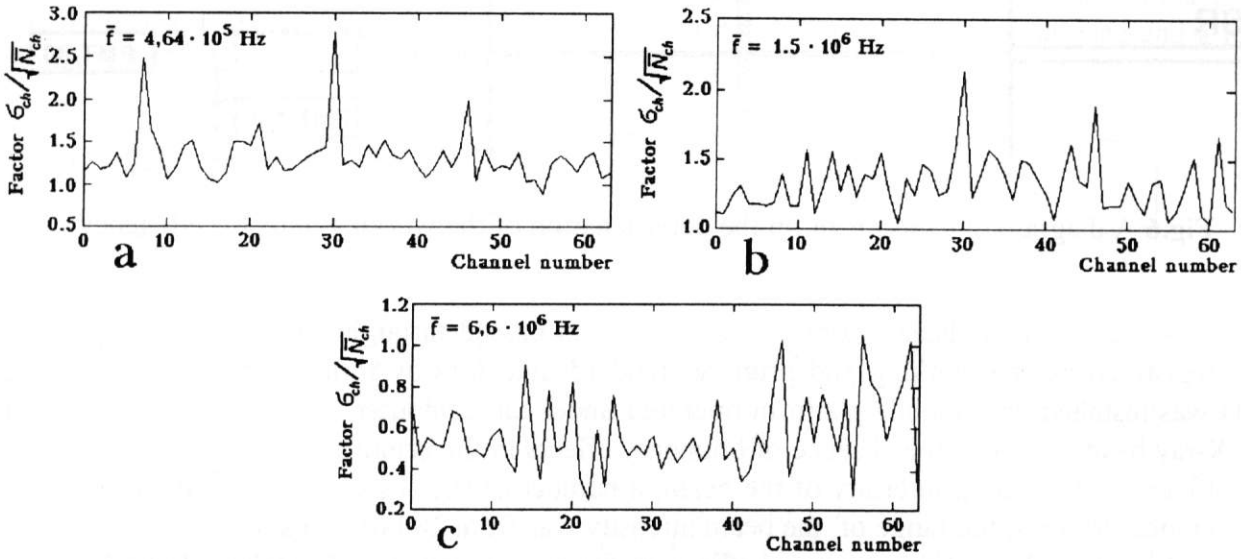

Fig. 7 Normalized counting spread $\sigma_{ch} \ / \ \sqrt{N_{ch}}$ for each of the 64 detector channels at different counting mean rates **f** and data acqusition times $\mathbf{t_a}$ (sampling interval $\mathbf{t_s}$=$\mathbf{t_a}$ + 4 ms): (a) f=0.46 MHz, $\mathbf{t_a}$=650 ms; (b) f=1.5 MHz, $\mathbf{t_a}$=130 ms; (c) f=6.6 MHz, $\mathbf{t_a}$=30 ms;

To reveal the frequences of counting disturbances, the time dependent data were collected. A time counting sequence and its Fourier spectrum for one of the detector channels are shown in Figs. 8a and 8b, correspondingly. The similar spectrum of a time sequence of the detector counting averaged at every sampling moment over 64 channels is given in Figure 8c. Both spectra are very similar one to another, and indicate the presence of disturbance factors with the characteristic frequencies of about 50, 85 and 92 Hz at the station or in the storage ring. However, as it follows from the counting spread measurements, the magnitude of these disturbances are rather low to have a noticeable effect on the detector counting.

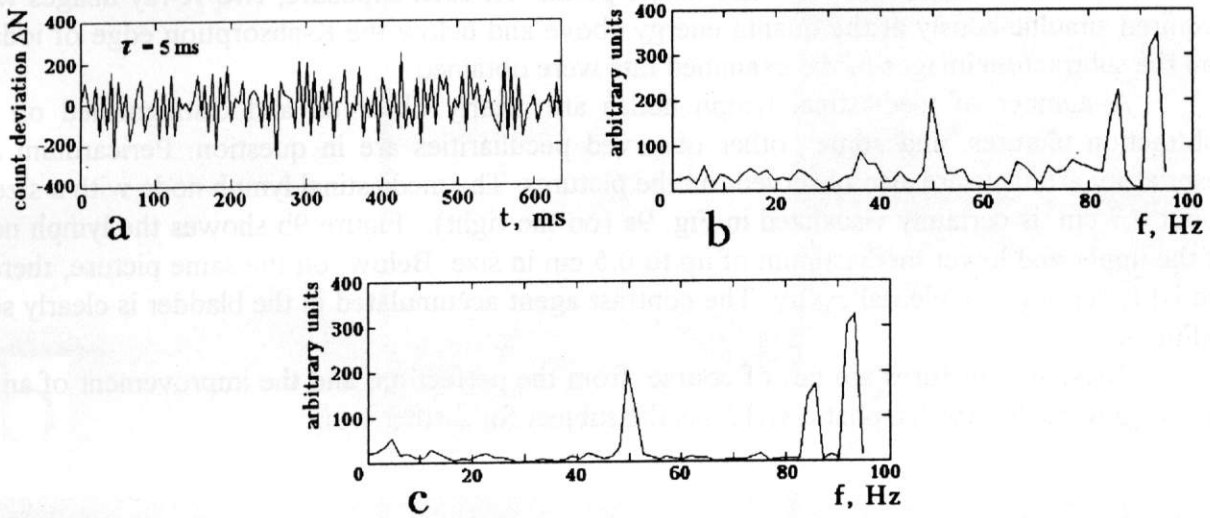

Fig. 8 Example of a time sequence of the detector channel counting (a) and its Fourier spectrum(b). The Fourier spectrum of a time sequence of the detector counting averaged over 64 channels (c). The count acqusition time is 1 ms, and the simpling interval is 5 ms.

After testing the detector performance, some X-ray imaging experiments were carried out. We used in these first experiments, as an object scanner, the translation unit with a stepping motor and with a 1 μm minimum step. Due to a low speed of this scanner, the total time for an X-ray picture acquisition was 1.5-2 min for the images of 64 * 128 points.

The existing problem associated with the presence of two SR emission points in the wiggler of VEPP-3, that leads to the image doubling, was overcome by using the special operation mode of the storage ring. This mode allowed to suppress the intensity of the second source by a factor of 8-10.

III. X-ray visualization of lymphatic system

In first experiments the contrasted lymph nodes of thorax of alive rats were examined. For investigations, we have chosen the unilamelar liposomes (ULL) with an iodine content [12]. Due to their good contrasting capability and harmlessness for the object, this preparation has been cleared for use in medical investigations by the Pharmacological Committee of Russia.

As previous investigations *in vitro* indicate, a concentration of contrast substances accumulated in lymph nodes of thorax does not exceed 1-2 % [6,7]. Though the test X-ray imaging experiments with a spatial resolution of 0.2 mm showed that water solution with an

iodine concentration as low as 0.25% were certainly detected inside a 2 mm diameter polyethilene tube, it was not evident beforehand that lymph nodes could be visualized inside a rat body.

Two alive rats of about 300 g weight were examined. They were etherized and after that the ULLs containing 40% of iodine were introduced into the pleural cavity of each rat. The exposures were taken over 4 and 6 hours after the initial etheric and further barbiturate narcosis when the ULLs content in the lymph nodes is the highest [7]. The X-ray pictures were taken with 0.4 mm and 0.12 mm spatial resolution, and with 128 lines of scanning, i. e. each picture consisted of 64 * 128 image points. At each exposure, two X-ray images were acquired simultaneously at the quanta energy above and below the K-absorption edge of iodine, and the subtraction images of the examined rats were obtained.

A number of mediastinal lymph nodes are clearly observed and distinguished on the subtraction pictures, and some other observed peculiarities are in question. Pericardium and respiratory artefacts are also observed on the pictures. The mediastinal lymph node with a size of about 0.7 cm is certainly visualized in Fig. 9a (on the right). Figure 9b showes the lymph node of the upper and lower mediastinum of up to 0.5 cm in size. Below, on the same picture, there is the ULL depot in the pleural cavity. The contrast agent accumulated in the bladder is clearly seen in Fig. 9c.

These first pictures are far, of course, from the perfection, and the improvement of an X-ray imaging quality for lymphatic system is the subject for further work

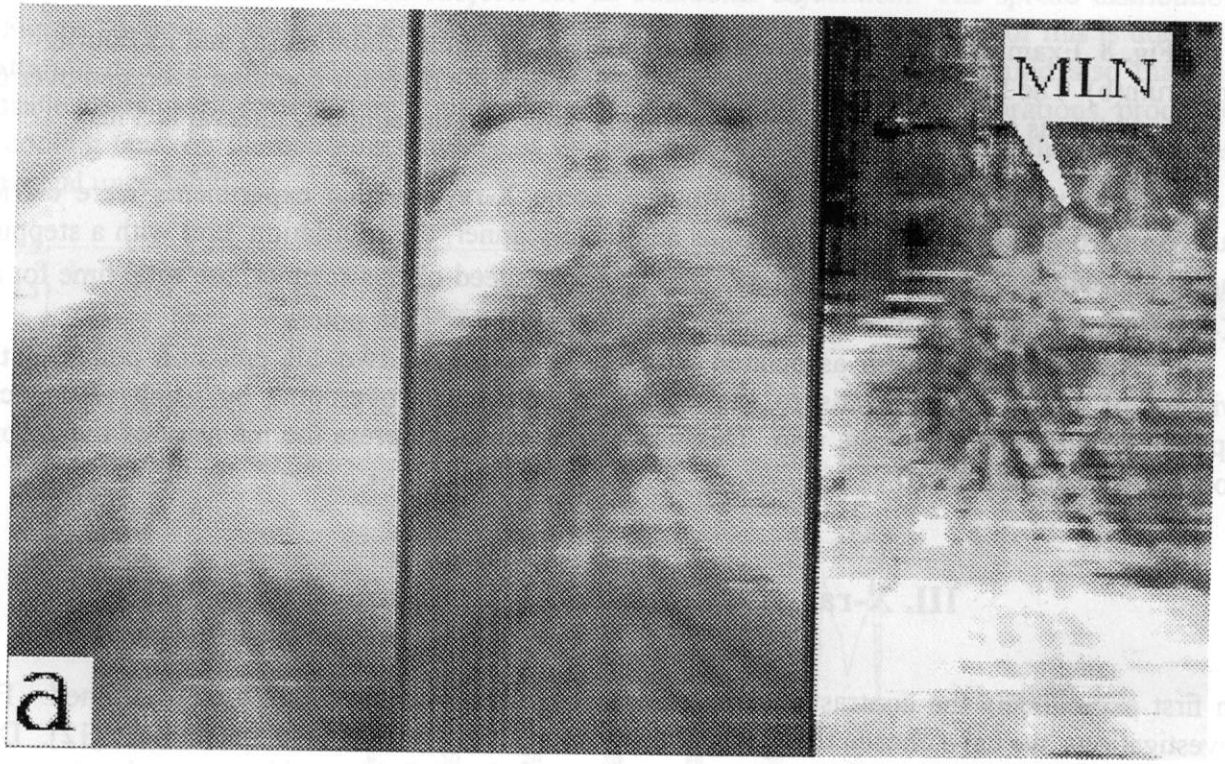

Fig.5 Usual, at qunta energy above (left) and below (center) the K-absorption adge of iodine, and subtraction (right) X-ray images of the thorax of livlng rats: MLN: mediastinal lymph node; ULL: ULL depot; B: bladder. Space resolution on the horizontal axis is 0.4 mm (a,b), 0.3 mm (c), space resolution on the vertical axis is 0.35 mm (a) and 0.4 mm (b,c).

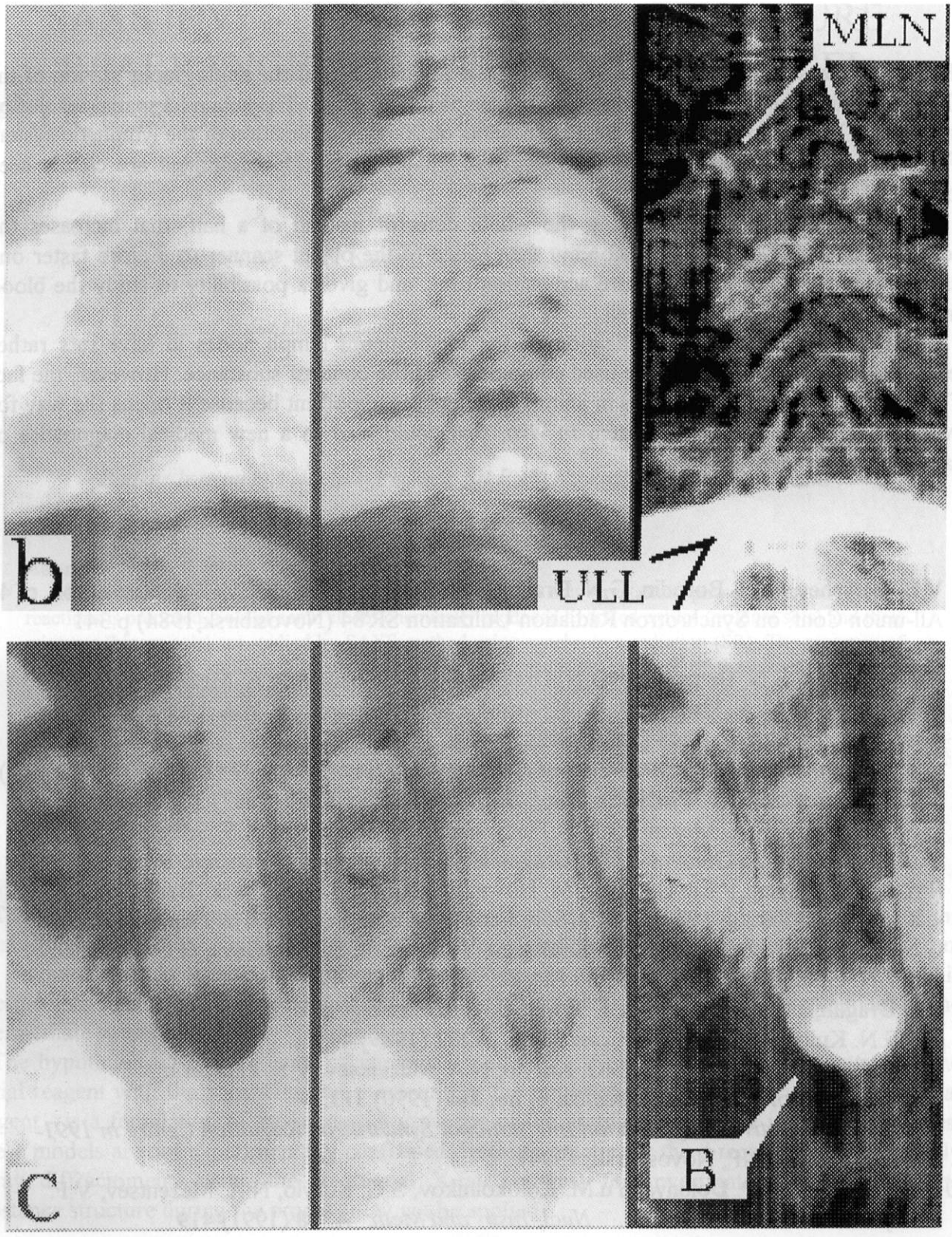

Fig. 5 (continued)

IV. Conclusion

The results of testing the double one-coordinate X-ray detector at the angiography station of the VEPP-3 storage ring show the good performance of the detector. The achieved spatial resolution as high as 0.1 mm allowed to start the experiments on X-ray visualization of the lymphatic system of alive animals. Two ways for further improvement of the station equipment are clearly seen now.

The first, it is commissioning the whole detector instead of a half, that increases the picture width by a factor of 2. Secondly, the change of the object scanner to a more faster one essentially reduces the X-ray picture acquisition time, and gives a possibility to study the blood circulatory system of animals as well.

The first results on visualization of the mediastinum lymph nodes in alive rats rather demonstrate the possibilities of the used equipment and the contrast substance. However, the fact of real observation of lymph nodes in animal body is very important because it opens the way for investigation of the lymphatic system *in vivo*, that could lead to a new medical diagnostics of many diseases at their early stages.

REFERENCES

1. V.B. Baryshev, Yu.I. Borodin, G.N. Dragun, G.N. Kulipanov and K.V. Zolotarev. Proc. of 4 All-union Conf. on Synchrotron Radiation Utilization SR'84 (Novosibirsk,1984) p.341 (in Russian).
2. Yu.I. Borodin, E.N. Dementyev, G.N. Dragun, G.N. Kulipanov, N.A. Mezentsev, V.F. Pindyurin, M.A. Sheromov, A.N. Skrinsky, A.S. Sokolov and V.A. Ushakov. *Nucl. Instr. and Meth.* **A246** (1986) 649.
3. G.N.Dragun and E.A.Bir. *Archieves of Histology and Embriology* , **7** (1986) 60 (in Russian).
4. N.A. Mezetsev and V.F. Pindyurin. *Nucl. Instr. and Meth.* **A261** (1987) 301.
5. G.N. Kulipanov, N.A. Mezentsev,V.F. Pindyurin, M.A. Sheromov, A.S. Sokolov, Yu.I. Borodin, V.A. Golovnev, G.N.Dragun and E.L. Zelentsov. *X-ray microscopy* (Proc. Intern. Symp.)/ Ed. D. Sayre, M. Howells, J. Kirz and H. Rarback (Berlin e.a.: Springer-Verlag, 1988), p.415 (Springer Ser. in opt. Sci./ Ed. Th. Tamir, v. 56).
6. G.N. Dragun,E.L. Zelentsov, K.V. Zolotarev, Yu.A. Zorin, L.F. Krylova, G.N. Kulipanov and V.N. Gorchakov. *Nucl. Instr. and Meth.* **A282** (1989) 493.
7. G.N.Dragun,E.L. Zelentsov, Yu.A. Zorin, O.A. Rozenberg, K.V. Zolotarev and G.N. Kulipanov. *Nucl. Instr. and Meth.* **A282** (1989) 495.
8. I.P. Dolbnya, G.N. Kulipanov, S.G. Kurylo, N.A. Mezentsev, V.F. Pindyurin and M.A. Sheromov. *Phisica Medica*, **6, no. 3-4** (1990) 313.
9. *Report on the Activities of Siberian International Synchrotron Radiation Centre in 1991-1992* (Preprint BINP, Novosibirsk, 1994).
10. V.P. Barsukov, I.P. Dolbnya, Yu.M. Kolokolnikov, S.G. Kurylo, N.A. Mezentsev, V.F. Pindyurin and M.A. Sheromov. *Nucl. Instr. and Meth.* **A308** (1991) 419.
11. E.N. Dementiev,I.P. Dolbnya, E.I Zagorodnikov, K.A. Kolesnikov, G.N. Kulipanov, S.G. Kurylo, A.S. Medvedko, N.A. Mezentsev, V.F. Pindyurin, V.G. Cheskidov and M.A. Sheromov. *Rev. Sci. Instrum.* **60, no. 7,** pt. II (1989) 2264.
12. *Liposomes: Application to X-radiology and radiobiology,* collected book (Leningrad State Post-graduate Training Institute for Phisicians, Leningrad, 1984) (in Russian).